International Journal of Hydrogen Energy 126 (2025) 386–395

Contents lists available at ScienceDirect

International Journal of Hydrogen Energy

journal homepage: www.elsevier.com/locate/he

An experimental study on the macroscopic behaviours of ammonia sprays in a constant volume chamber

Li Shen *, Felix Leach

Department of Engineering Science, University of Oxford, 17 Parks Road, Oxford OX1 3PJ, Oxfordshire, UK

ARTICLE INFO

Keywords:
Ammonia
Spray morphology
High speed backlit imaging
Flash boiling
Spray collapse

ABSTRACT

Green ammonia is a promising alternative fuel for future thermal propulsion systems. In its liquid form, ammonia provides an energy density by mass comparable to conventional hydrocarbon fuels. Already high levels of mass-production and widely available existing infrastructure enable a smooth transition from fossil fuels to ammonia on the supply side. However, on the application side, the evaporation and mixing processes of liquid ammonia in air, which are known to have significant impacts on the energy release and resulting emissions, differ notably from those of fossil fuels. Hence, existing spray models may not be applicable to liquid ammonia injection. This calls for a comprehensive experimental study of ammonia sprays under a variety of relevant test conditions in order to understand the nature of such processes and for model validation. In this work, liquid ammonia was injected into a constant volume chamber from a direct injector at three injection pressures (100 bar, 150 bar and 200 bar) at ambient pressures varying from 1 bar to 10 bar, with an increment as low as 0.5 bar. This selection of ambient pressures covers a range of flash boiling to non-flash boiling conditions. It was found that the flash boiling regime of ammonia sprays are much lower than its saturation pressure, indicating there exists a strong cooling effect presumably due to its high latent heat of evaporation. Also, the spray collapse phenomenon was observed in ammonia sprays, and the spray collapse point was determined by a morphological study. These tests provided a comprehensive validation dataset for spray models.

1. Introduction

Ammonia (NH_3), which contains no carbon, is widely recognised as a suitable alternative to diesel and heavy fuel oil, which currently power a number of sectors, including maritime transportation, energy storage, and stationary power generation using internal combustion engines and gas turbine engines [1]. Ammonia is one of the energy vectors under serious consideration to decarbonise these sectors, which are significant emitters of carbon dioxide. For example, the marine sector emits over 1 billion tonnes of carbon dioxide each year [2], which represents ≈ 2.9% of the global total anthropogenic greenhouse gas emissions per year. Ammonia is one of the most-produced chemicals in the world, primarily for use as a fertiliser, via the Haber-Bosch process with 176 million tonnes being produced in 2019 [3]. Ammonia can be produced entirely from renewable resources using electrolysis and renewable electricity [1]. Ammonia is an excellent energy carrier, it has amongst the highest energy densities of any energy vector not containing carbon, including around 10 times higher than lithium-ion batteries and 30% higher than liquid hydrogen (which must be liquefied cryogenically, a very energy intensive process) [4]. Indeed, ammonia contains 50% more hydrogen by volume than liquid hydrogen [5,6]. Ammonia, on the other hand, can be stored as a liquid at a moderate pressure (above 8.5 bar at 20 °C [5,7]). Much of the work on ammonia in internal combustion engines has focused on gaseous ammonia injection [8–10]. This has numerous advantages including superior air–ammonia mixing locally, simplicity, and the ability to use injection equipment and engines previously developed for natural gas, as ammonia gas jets behave quite similarly to natural gas jets [11]. However, gaseous ammonia injection, particularly if injected into the inlet port (port fuel injection), substantially reduces the power density and volumetric efficiency of an internal combustion engine [12].

On the other hand, directly injecting (DI) ammonia as a liquid has advantages such as using the higher momentum of liquid ammonia droplets to improve air–ammonia mixing globally (fuel–air mixing is known to have a significant influence on emissions formation in internal combustion engines [13]) and enabling a much higher power density (liquid ammonia has a density ≈ 850 times higher than gaseous ammonia). Nevertheless, liquid ammonia has challenges evaporating in the combustion chamber due to its high latent heat of vaporisation, which can result in spray droplets still being present during

* Corresponding author.
E-mail addresses: sam-li.shen@eng.ox.ac.uk (L. Shen), felix.leach@eng.ox.ac.uk (F. Leach).

https://doi.org/10.1016/j.ijhydene.2025.03.347
Received 25 November 2024; Received in revised form 19 February 2025; Accepted 24 March 2025
Available online 10 April 2025

combustion, leading to less efficient combustion and higher emissions. Therefore, there is a significant body of work which needs to be done to understand the breakup and evaporation of liquid ammonia sprays under conditions which are representative of those found in an internal combustion engine.

The spray atomisation of hydrocarbon fuels, on the other hand, has been comprehensively studied for many years, with the aim of enhancing spray–air mixing within the combustion chamber and distributing the injected mass uniformly before ignition [14]. Among many methods attempted, flash boiling atomisation is recognised as a promising mechanism to generate finer droplets and potentially achieve a more uniform mixture, however with the risk of smaller droplets having less momentum leading to a less uniform mixture [15]. The concept of flash boiling sprays is closely related to pressure gradient, in-nozzle cavitation and primary breakup of the droplets near nozzle exit, which has been described in detail in many review articles [14,16,17], and a short summary is provided here. The high speed flow induced by the large pressure gradient between the fuel upstream in the supply line (at injection pressure) and downstream at the nozzle exit (at ambient/chamber pressure), when passing through some in-nozzle features (such as sharp corners), may encounter a local pressure drop. This prompts a liquid-to-vapour phase change and gaseous fuel bubbles starts to form within the liquid stream (cavitation). When ambient pressure further drops, usually to below the saturation vapour pressure of the injected fluid, cavitation occurs much more readily, causing droplets to break up from their interior immediately after leaving the nozzle (flash boiling). The resulting external plume undergoes a more rapid radial expansion than a non-flash boiling case [18]. For a multi-hole injector, when the expanded adjacent plumes are close enough to each other, a mechanism similar to the Coandă effect [19] occurs — the adjacent high speed plumes create an enclosure that has a lower pressure than the pressure on the side that is open to the nearly-quiescent surrounding gases, and this pressure difference eventually led to the merge of multiple plumes into a single one. This drastic change in spray morphology is referred as "spray collapse", and it is one of the key features observed before in multi-hole hydrocarbon sprays [20–22].

Recently, researchers have started to perform experimental studies on the morphological behaviours of liquid ammonia sprays, which has a different fluid property from hydrocarbon or alcohols. Pelé et al. [23] undertook one of the first studies on liquid ammonia sprays (comparing them to gasoline and ethanol sprays) using a repurposed gasoline direct injection (GDI) fuel system. They found that at most conditions, ammonia sprays exhibited substantially different behaviour to gasoline and ethanol (which behave similarly) — for example having a longer penetration length and a smaller spray cone angle. In addition, it was reported that ammonia spray morphology has a much higher dependence on the ambient conditions compared to gasoline and ethanol. Cheng et al. [24] also explored a repurposed gasoline direct injection (GDI) injector using liquid ammonia. They found that ammonia sprays mixed more rapidly than air compared to methanol or ethanol and that the ammonia sprays had higher spray angles. They also reported substantial sensitivity to the ambient conditions, similar to what was found by Pelé et al. [23]. Colson et al. [25], similarly using a repurposed GDI injector, found a transition region into flash boiling that was controllable, to some extent, with nozzle design. In addition to repurposed GDI injectors, ammonia sprays have also been studied from repurposed diesel injectors. Fang et al. [26] used a diesel injector with ammonia, at much higher pressures than the previous GDI studies (up to 1000 bar) and found that under flash boiling conditions, the penetration speed of the spray tip substantially reduced. Li et al. [27] also used a diesel injector at high injection pressure (300 bar) and investigated the effects of superheated degree and pressure ratio (either ambient-to-saturation or its reciprocal) on the characteristics of ammonia sprays. In their comprehensive tests, they found that the flashing regions of ammonia sprays can be split into different regions based on the morphological behaviour under various pressure ratios, which is similar to hydrocarbon sprays [20]. However, the spray collapse phenomenon was not reported in their work as the setup was a single hole injector.

In this paper, a multi-hole GDI injector from a production vehicle combustion system is repurposed to inject liquid anhydrous ammonia at room temperature (around 20 °C) into a constant volume chamber. The injector operates at three injection pressures (100 bar, 150 bar and 200 bar) and at a fixed injection duration of 2 ms. The ambient (chamber) pressure is set between 1 bar to 10 bar with a minimum increment of 0.5 bar between neighbouring test points. The spray is recorded by a high-speed diffuse backlit imaging (DBI) technique at 10 kFPS. The effects of ambient pressures and injection pressures on ammonia sprays are examined. Spray morphological behaviour is quantified by macroscopic parameters such as tip penetration length and spray cone angle. Flash boiling region and spray collapse point of ammonia sprays are identified. The current tests provide a comprehensive data set for model validation.

2. Methodology

2.1. Test rig

Measurements of ammonia sprays were undertaken in a constant volume chamber filled with nitrogen at various ambient pressures. This chamber and the setup has been comprehensively described in previous work [28], but a summary and a schematic (Fig. 1) are given here, for convenience. The chamber has optical access along three axes, facilitated by five 80 mm viewable diameter fused silica (quartz) windows, two pairs on the side and one at the bottom.

The injector used in this work is a Bosch six-hole injector, which has been previously described in [29,30]. This injector originated as a gasoline direct injector for a production light-duty vehicle combustion system but has since been repurposed to inject liquid anhydrous ammonia, including by replacing the original o-ring seal with EPDM, a material which is compatible with ammonia. A recent measurement using an X-ray computed tomography (XCT) technique provided further details of the geometrical parameters of its nozzles. It has a distinctive spray pattern, with four plumes heading generally downwards (axially, nozzle holes 23° w.r.t. its axis) and two heading in a more orthogonal (radially, nozzle holes 48° w.r.t. its axis) direction. All six holes are counterbored — upstream 210 μm diameter and 300 μm long, and downstream 440 μm diameter and 300 μm long. All of these parameters are subject to an error of ±2° or ±10 μm. The injector was driven with a driver provided by its manufacturer. The setting of injection duration as well as the synchronisation among the camera, laser droplet sizer and injector were achieved with a Berkeley Nucleonics Corporation BNC 725 pulse/delay generator.

Anhydrous liquid ammonia was pressurised with a Heypac GX40 series pump before feeding to the injector, and its pressure was measured with an in-line GEMS 3100 series transducer. The chamber was pressurised with nitrogen gas, whose pressure was measured with another GEMS 3100 series pressure transducer mounted at the bottom of the chamber. All data and individual trigger of each device, were recorded by a PicoScope 6000E Series data logger at 100 kHz.

Spray images were recorded by a high speed camera (Photron FASTCAM-1024PCI 100K), operated in these tests at 10 000 FPS with a resolution of 256 pixel × 272 pixel and an exposure time of 10 μs. The images taken were shadowgraph images by back-illuminating the spray with a white (i.e., broadband) LED shining through a diffusing screen giving a uniform backlighting to the images. The resulting pixel resolution in each image was 0.25 mm pixel^{-1}, corresponding to a maximum error of 1.25% in all images.

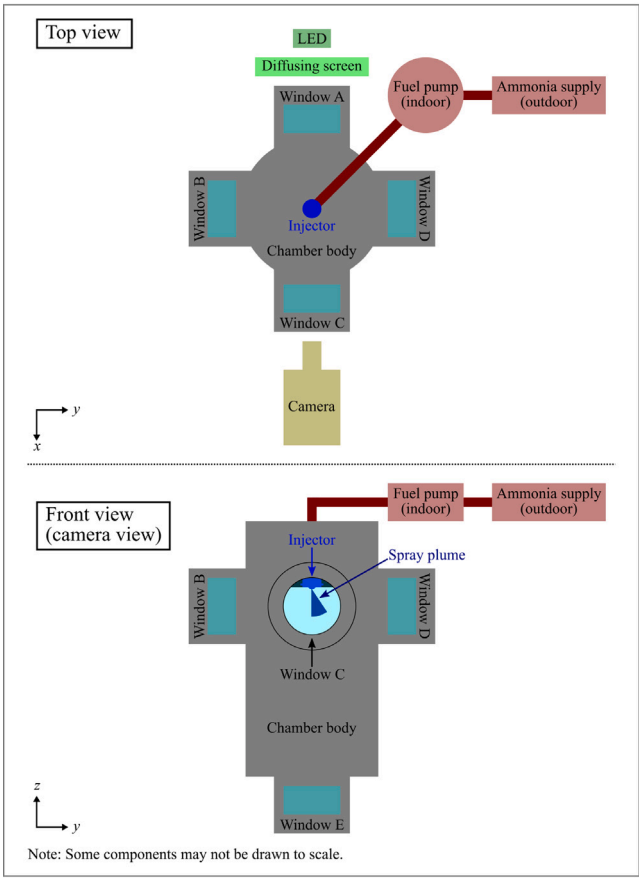

Fig. 1. Schematic of the experimental setup in two views.

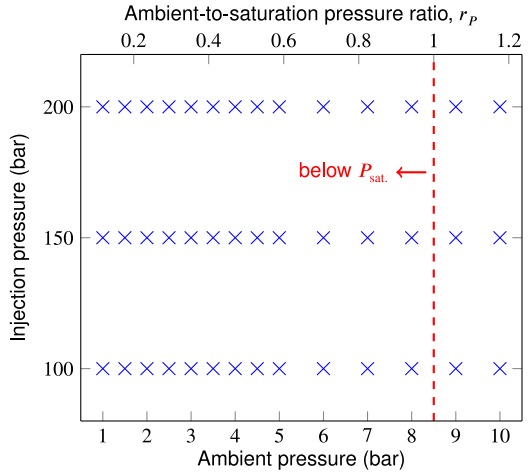

Fig. 2. Test matrix. The blue markers show the test points, and the red dashed line illustrates the saturation vapour pressure ($P_{sat.}$) of ammonia under the test temperature (20 °C).

2.2. Test conditions

The test points in this paper were taken at three injection pressures ($P_{inj.}$, at 100 bar, 150 bar and 200 bar) and in a range of ambient pressures ($P_{amb.}$, 1 bar to 10 bar with various increments as small as 0.5 bar). The test matrix is illustrated in Fig. 2 — each blue marker refers to a test point, and the red dashed line shows the saturation vapour pressure ($P_{sat.}$) of ammonia at the test temperature (8.5 bar at 20 °C [5]). The top horizontal axis labels the (dimensionless) ambient-to-saturation pressure ratio, defined as [20]:

$$r_P = \frac{\text{ambient pressure}}{\text{saturation vapour pressure}} = \frac{P_{amb.}}{P_{sat.}}$$

The ambient pressure is lower than the saturation vapour pressure if r_P falls below 1, and in this case flash boiling is more likely to occur.

At each point, the injector was triggered at 1 Hz to perform 20 consecutive shots at 2 ms injection duration. After each test, the chamber was vented completely and purged using nitrogen for at least five minutes, before it was recharged by nitrogen to the target ambient pressure for the next test point.

2.3. Image post processing and macroscopic spray parameters

Fig. 3(a) shows an example raw image taken at 1.0 ms after the start of injection (ms aSOI). The injection pressure was at 150 bar and the ambient pressure being 9 bar. The two radial plumes pointed toward the camera (outwards the paper). To isolate spray plumes from stationary chamber features for further analysis, ten blank images without spray, such as Fig. 3(b), were recorded before each shot and, when they are subtracted from the raw images (Fig. 3(a)), the resulting background subtracted image (Fig. 3(c)) contains the spray plumes only.

These images (Fig. 3(c)) are then used to compute the macroscopic spray parameters using an algorithm based on the SAE J2715 standard [31,32], summarised as follows and illustrated in Fig. 4 (a zoomed-in plot of Fig. 3(c)):

Tip penetration length The injector tip is labelled by a red dot (Point O), and among all the darker pixels that show the presence of spray plume (liquid), Point P (blue dot) is the furthest away from the injector tip. Hence, the tip (liquid) penetration length is defined by the length of line segment OP.

Spray cone angle A circle centred at the injector tip with a 5 mm radius can be drawn in each image (illustrated by the orange dashed circle in Fig. 4), and it intersects the spray plume at Point A (orange triangle marker) and Point A' (orange rectangle marker). These two points define the plume edges at 5 mm away from the injector tip. A similar procedure was repeated at a 15 mm radius (teal dashed circle) to obtain the plume edges further downstream, denoted Point B (teal triangle marker) and Point B' (teal rectangle marker). The spray cone angle is thus defined by the angle between line segments AB and A'B' (purple dash-dotted lines). It should be noted that the spray must have penetrated for a long enough distance (at least 15 mm, preferably longer for a stable result) away from the injector tip to enable the calculation of spray cone angle.

3. Results

3.1. Observations from raw images

Fig. 5 illustrates the ammonia spray images recorded at 150 bar injection pressure at different timings and ambient pressures. Each row shows the images recorded at the same timing (value shown in the first column), and the images in each column are recorded under the same ambient pressure (i.e., the same test point). The ambient pressures ($P_{amb.}$) and the corresponding ambient-to-saturation pressure ratios (r_P) are labelled at the top of each column. The injector tip defines the origin of each plot.

As the spray leaves the nozzle, the plumes gradually penetrate in the chamber. At 9 bar (column (a)), all six plumes from the six-hole injector can be seen, albeit that there are some inevitable overlay among them in these line-of-sight images due to the viewing angle of the camera. The four axial plumes roughly have an equal penetration, which matches with the injector design as all these holes have the same internal diameter and the same angle with respect to the injector axis (z axis). The two radial plumes point more out of plane, so they appear to have a shorter penetration length when imaged in this view.

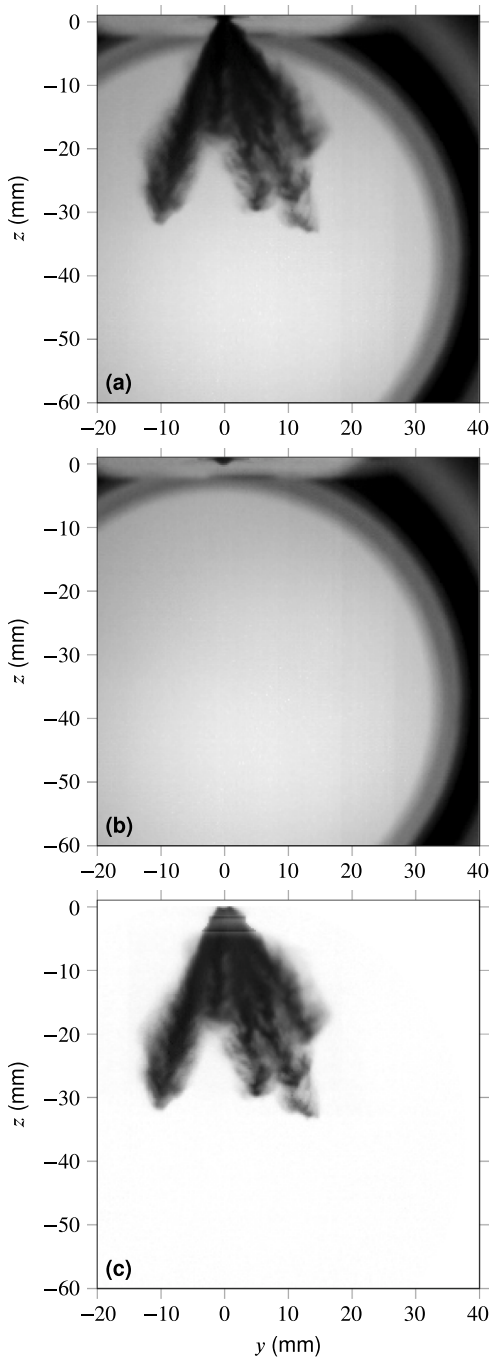

Fig. 3. (a) An example raw image recorded at 1.0 ms aSOI, at 150 bar injection pressure and at 9 bar ambient pressure; (b) a blank image taken before the same injection shot as (a), used as a background; (c) background subtracted image of (a).

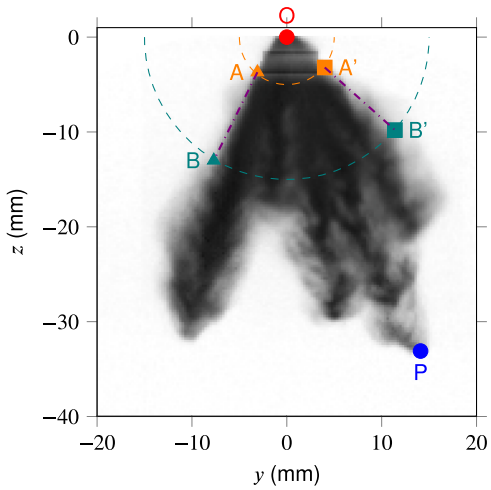

Fig. 4. A zoomed-in plot of Fig. 3(c), superposed by labels illustrating the SAE J2715 standard. Point O: injector tip; Point P: furthest point away from Point O in the plume; Points A and A': plume edges at 5 mm away from Point O; Points B and B': plume edges at 15 mm away from Point O.

Under this pressure (9 bar), the plumes from each individual hole are clearly separated and the spray is non-flash boiling. The ambient pressure is still higher than the saturation vapour pressure ($r_P > 1$), the evaporation of the droplets only occurred at their outer edge, and within such a short period of time (from 0.6 to 1.8 ms aSOI), there is limited ambient gas intrusion so the evaporation mainly happened near the plume boundaries.

When the ambient pressure drops (say, 3 bar in column (b)), as the density of the surrounding gases (mainly nitrogen) reduces — density of an ideal gas such as nitrogen is proportional to pressure at the same temperature — there is less drag applied on the penetrating spray, and this results in a longer penetration at the same timing. For instance, at 1.2 ms aSOI, the plume has not yet reached the line $z = -40$ mm when the ambient pressure is at 9 bar (plot (a3)), but it has exceeded the line $z = -45$ mm at 3 bar ambient pressure (plot (b3)). Despite that the ambient pressure is below the saturation vapour pressure ($r_P < 1$), at 3 bar ambient pressure, the plumes are still separated in the images (column (b)). However, considering that the ambient pressure is much lower than the saturated vapour pressure ($r_P = 0.35$ when $P_{\text{amb.}} = 3$ bar), a flash-boiling phenomenon [14] may have occurred. In addition to the gradual evaporation near plume boundaries, the droplets also undergo a more rapid cavitation process — bubbles containing evaporated (gaseous) ammonia are formed interior of the droplets and prompt the breakup (or even an exposure) of the original droplets into smaller ones.

The effect of flash boiling is not be obviously seen in spray images until the ambient pressure further dropped to 2 bar (column (d)), at which a so-called "spray collapse" phenomenon is observed — all six plumes merge into a single one as soon as the spray leaves the nozzle, and only a single stream is visible in the images throughout the injection event. As discussed in the Introduction section, the spray collapse is caused by the pressure difference between the sides of multiple high-speed plumes. The spray collapse is usually seen as an indication of the (flare) flash-boiling region in multi-hole hydrocarbon sprays [20–22], and it is in this paper observed in ammonia sprays as well.

When the ambient pressure is slightly higher, at 2.5 bar (column (c)), the images show a partially collapsed plume — the plumes merge to two plumes instead one at earlier timings (before 1.2 ms aSOI, the third row) when the flash boiling has just begun and the plumes has not expanded enough. And, at a later timing (for instance at 1.8 ms aSOI, the fifth row) the expansion of the individual plumes finally merge the two streams into a single one. This shows a transition between a milder flash boiling regime without spray collapse (observed at medium ambient pressures) and a flare flash-boiling regime with spray collapse (observed at low ambient pressures).

Under all the tested conditions, the complete spray collapse is only observed for ambient pressures lower or equal to 2 bar, or, more specifically, at 2 bar, 1.5 bar and 1 bar ambient pressures — the images for the latter two conditions are not shown here for brevity but they look similar to the ones at 2 bar (column (d) in Fig. 5) and both have only one stream visible. This corresponds to an ambient-to-saturation pressure ratio (r_P) below 0.23, and such a value, known as the "spray collapse point", is lower than the one for hydrocarbon fuels (0.3) reported in

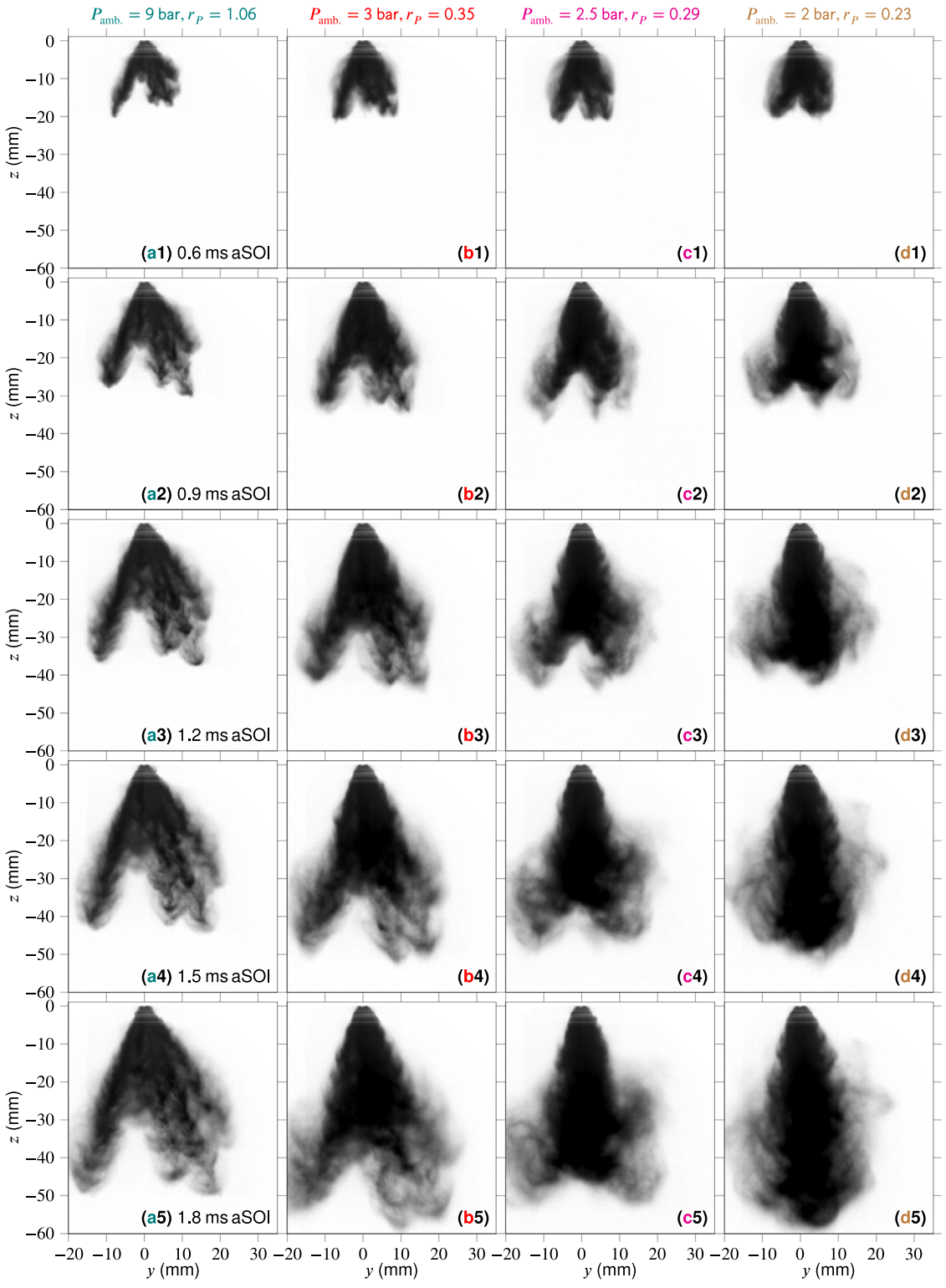

Fig. 5. Spray images recorded at 150 bar injection pressure at different timings (rows) and ambient pressures (columns).

Zeng et al. [20]. This may be resulted from an evaporative cooling effect due to the excessively higher specific latent heat of ammonia (more than three times larger than iso-octane [5]). The evaporation of the liquid ammonia droplets reduces the surrounding temperature significantly [33], and hence the local saturation vapour pressure, evaluated at the local temperature of the surroundings of the spray, will be much lower than the value obtained from the injection temperature (fuel temperature). As a result, the local ambient-to-saturation pressure ratio, which will drive evaporation behaviour, is likely to be higher than the reported values.

3.2. Temporal evolution of macroscopic spray parameters

The macroscopic spray parameters derived from the spray images give a quantitative insight of spray behaviour under a variety of test conditions. Fig. 6 reports the tip penetration length and spray cone

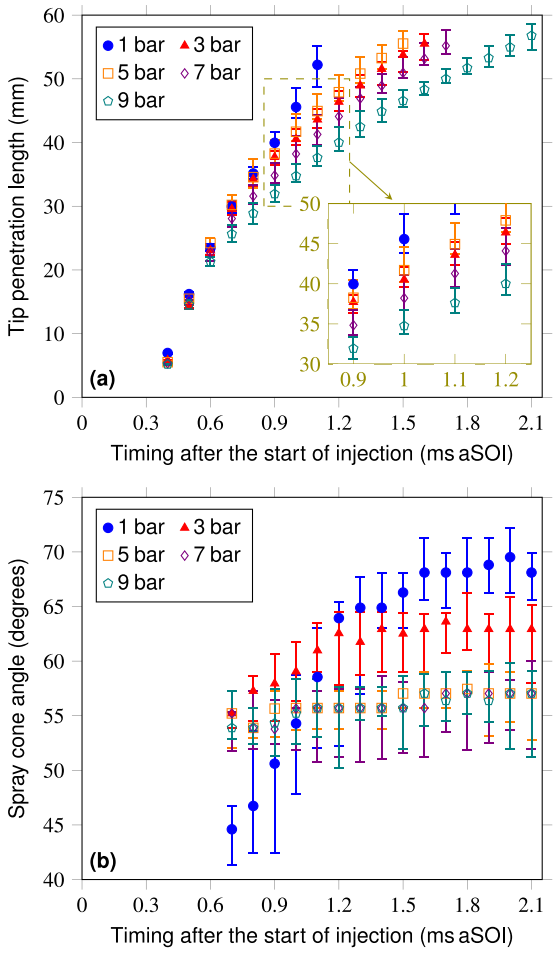

Fig. 6. Macroscopic spray parameters as functions of time at 150 bar injection pressure. (a) Tip penetration length (with a zoomed-in plot) and (b) spray cone angle.

angle as respective functions of time (in a unit of ms aSOI) at 150 bar injection pressure and under five ambient pressures ranging 1 bar to 9 bar at a 2 bar increment. Each marker labels the median value of the results from 20 consecutive shots in a single test run, and the lower and upper bounds of the error bars are the 10% and the 90% percentiles, respectively.

At all tested conditions, the tip penetration lengths (Fig. 6(a)) increase monotonically with respect to timing as the spray travels away from the injector tip, until the values exceed the viewable limit of the window (above 60 mm). In line with the observations from the images (Fig. 5), at any given timing, the penetration length is shorter at 9 bar ambient pressure (teal markers in Fig. 6(a), column (a) in Fig. 5) than those at lower ambient pressures such as 3 bar (red markers in Fig. 6(a), column (b) in Fig. 5) or 1 bar (blue markers in Fig. 6(a), images not shown for brevity). Such a trend is again expected as due to the higher drag induced by higher density at higher ambient pressure. Also, the spray collapse appeared at extremely low ambient pressures (such as at 1 bar), despite it drastically alters the plume shape (seen before in Fig. 5), does not change the trend that higher ambient pressure (density) normally leads to a shorter penetration length.

Interestingly, this trend reverses at ambient pressures in the middle of the range — when ambient pressure reduced from 5 bar (orange markers in Fig. 6(a)) to 3 bar (red markers). The penetration lengths are about 3.5 percent longer at 5 bar compared to the ones at 3 bar when the spray has travelled for a sufficient distance within the chamber (after 0.9 ms aSOI). This may be a result from two competing mechanisms — the decreased ambient pressure prompts the spray to penetrate further in the chamber as there is less drag (owing to a lower ambient density), but in the meantime it also reduces the ambient-to-saturation pressure ratio (r_P) and enhances the flash boiling of the droplets within the plume. The latter leads to a more rapid evaporation of the droplets and, since the backlit imaging technique used in this paper only captures the liquid part of the plume, the liquid tip penetration length is reduced. In this medium ambient pressure range (around 3 bar), the enhanced evaporation is more dominant than the reduced drag, resulting in an overall shorter tip penetration length when ambient pressure is lower.

The spray cone angle, on the other hand, does not vary much after the spray left the nozzle at higher ambient pressures. As shown in Fig. 6(b), when plotted as a function of timing (orange markers at 5 bar, purple markers at 7 bar and teal markers at 9 bar), the spray cone angle is always at 56° ± 2° regardless of timing.

At lower ambient pressures, however, the spray cone angle increases at a later timing as a result of plume expansion owing to a stronger evaporation mechanism under these conditions. At 3 bar (red markers in Fig. 6(b)), the value is similar to the value at higher pressures (about 56°) at 0.7 ms aSOI, but it increases to 63° within the next 0.5 ms (at 1.2 ms aSOI) and the value remains stable subsequently. The plume expansion is much more obvious under extremely low ambient pressures when spray collapse occurs — at 1 bar (blue markers), the spray cone angle increases rapidly from below 45° at 0.7 ms aSOI to 65° at 1.2 ms aSOI, and increases gradually to 68° after 1.6 ms aSOI. This suggests that in this flare flash boiling region, the spray is firstly narrowed (from the side) due to the plume merging, and at a later timing, the merged plume starts to expand rapidly in a radial direction under a combined effect of low ambient density (low drag) at its outer boundary and the violent droplet breakup and evaporation happening in its interior.

3.3. Spray morphological behaviour in three regions of ambient pressures

These findings suggest that ambient pressure (or equivalently, at a fixed saturation pressure, the ambient-to-saturation ratio r_P) has a profound effect on morphology of ammonia sprays. The effect of ambient pressures can be viewed in a more detail from another perspective — when the macroscopic spray parameters are instead reported as respective functions of ambient pressures (and r_P labelled on the top axis) in Fig. 7 (for tip penetration lengths) and in Fig. 8 (for spray cone angles) at various timings. In addition to the test points at 150 bar injection pressure discussed previously in Fig. 6, these two figures also show the macroscopic spray parameters at all three injection pressures – at (a) 100 bar, (b) 150 bar and (c) 200 bar, as well as in a finer test point selection (0.5 bar increment for ambient pressure 1 bar to 5 bar).

For instance, Fig. 7(b) further reveals that, among all tested conditions at 150 bar injection pressure, the penetration length is maximised when $r_P = 0.53$ (4.5 bar ambient pressure), and from Fig. 8(b), the increase of spray cone angle (an indication of plume expansion due to flash boiling) also starts when ambient pressure falls below this pressure. This suggests that, from a morphology point of view, the relative importances of ambient drag (dynamic breakup, dominant at higher ambient pressure) and evaporation (thermal breakup, dominant at medium ambient pressure) swap when $r_P < 0.53$ (or ambient pressure reduces to below 4.5 bar). The strong evaporation at low ambient pressures prevents the plumes from penetrating further and also expands each plume in its radial direction (i.e., wider and larger cone angle).

When the ambient pressure further drops (below or equals to 2 bar, or $r_P < 0.23$), as illustrated before in Fig. 5(d), the spray collapses into a single plume, and such a drastic change leads to different aerodynamic properties. The penetration length (Fig. 7(b)) of the merged plume shortens as ambient pressure reduces — a phenomenon similar to the observations at higher ambient pressures (above 4.5 bar, or $r_P \geq 0.53$). However, the change of its spray cone angle (Fig. 8(b)) seems to be less ordered — the values fluctuate both with respect to ambient pressures and in different timings.

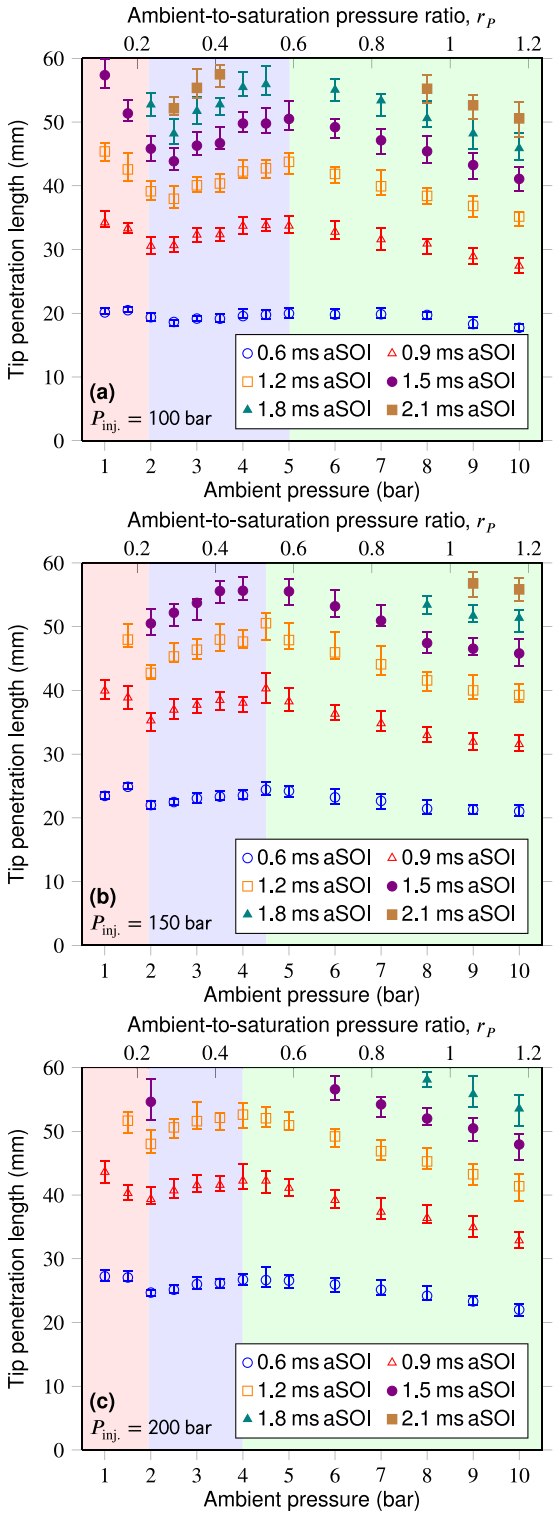

Fig. 7. Tip penetration length at various timings as a function of ambient pressure at three injection pressures. (a) At 100 bar, (b) at 150 bar and (c) at 200 bar.

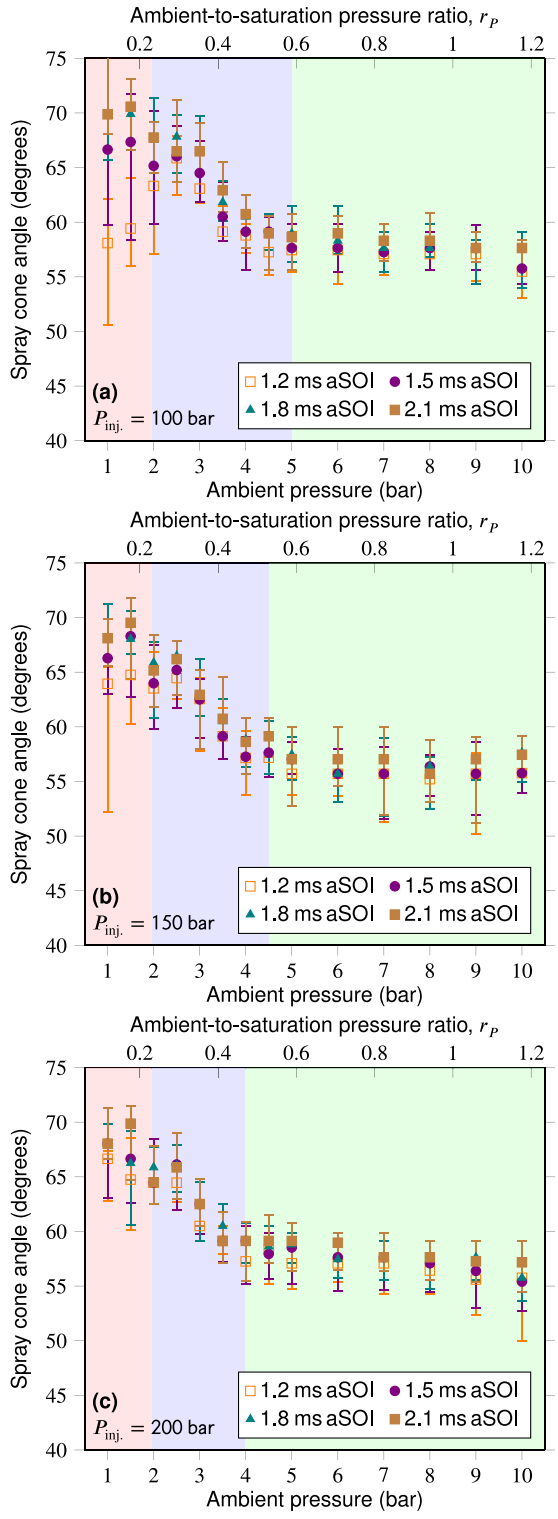

Fig. 8. Spray cone angle at various timings as a function of ambient pressure at three injection pressures. (a) At 100 bar, (b) at 150 bar and (c) at 200 bar.

3.4. Spray morphological behaviour under different injection pressures

Inspired by the above findings at 150 bar injection pressure, one may split the tested conditions into three regions based on dominant mechanisms affecting the spray morphological behaviour, as summarised in Table 1. At high ambient pressures, the drag from the dense and quiescent ambient gas dominates, and the penetration length shortens at higher ambient pressure (density) while the cone angle remains almost constant. At medium ambient pressures, the evaporation of droplets and their thermal breakup becomes more important, so the trend of penetration length reverses — shorter penetration length is observed at lower ambient pressure, and in the meantime the cone angle increases due to plume expansion. In this evaporation dominant region, the flash boiling is mild and plumes from each hole are still

Table 1
Summary of the three regions of spray morphological behaviour at 150 bar injection pressure.

Region	Ambient-to-saturation pressure ratio (ambient pressure range)	Penetration length trend	Cone angle trend
Drag dominant	$r_P \geq 0.53$ ($P_{amb.} \geq 4.5$ bar)	Decrease as $P_{amb.}$ ↑	Almost constant
Evaporation dominant or mild flash boiling	$0.23 < r_P < 0.53$ ($2.0 < P_{amb.} < 4.5$ bar)	Increase as $P_{amb.}$ ↑	Decrease as $P_{amb.}$ ↑
Spray collapse or flare flash boiling	$r_P \leq 0.23$ ($P_{amb.} \leq 2.0$ bar)	Decrease as $P_{amb.}$ ↑	Highly fluctuating

Table 2
Ranges of the three regions of spray morphological behaviour and evaporation mechanisms at different injection pressures.

Region	Evaporation mechanism	$P_{inj.} = 100$ bar	$P_{inj.} = 150$ bar	$P_{inj.} = 200$ bar
Drag dominant	External heat transfer	$r_P \geq 0.59$ ($P_{amb.} \geq 5.0$ bar)	$r_P \geq 0.53$ ($P_{amb.} \geq 4.5$ bar)	$r_P \geq 0.47$ ($P_{amb.} \geq 4.0$ bar)
Evaporation dominant or mild flash boiling	Both	$0.23 < r_P < 0.59$ ($2.0 < P_{amb.} < 5.0$ bar)	$0.23 < r_P < 0.53$ ($2.0 < P_{amb.} < 4.5$ bar)	$0.23 < r_P < 0.47$ ($2.0 < P_{amb.} < 4.0$ bar)
Spray collapse or flare flash boiling	Superheated evaporation	$r_P \leq 0.23$ ($P_{amb.} \leq 2.0$ bar)	$r_P \leq 0.23$ ($P_{amb.} \leq 2.0$ bar)	$r_P \leq 0.23$ ($P_{amb.} \leq 2.0$ bar)

separated. At low ambient pressures, the spray enters the flare flash boiling region and the expanded plume finally merges, leading to the spray collapse phenomenon. The penetration length of merged plume again shortens at higher ambient pressures, and a large fluctuation in cone angle is observed under different ambient pressures as well as at different timings. The separation of regions is additionally shown as coloured background in Figs. 7 and 8 — green for the drag dominant region, blue for the evaporation dominant region and red for the spray collapse region.

The injection pressure has an effect on the spray morphological behaviour, too. At lower injection pressures, there is less momentum carried by the injected fluid. As a result, at the same timing and under the same ambient pressure, the tip penetration lengths at 100 bar injection pressure (Fig. 7(a)) are shorter than those at 150 bar (Fig. 7(b)) and 200 bar (Fig. 7(c)) injection pressures. For instance, at 1.5 ms aSOI (purple markers) and 5 bar ambient pressure, the tip penetration length is about 50 mm when the injection pressure is at 100 bar, while for 150 bar injection pressure the value is about 55 mm and for 200 bar injection pressure the plume tip has exceeded the viewable limit of the window (above 60 mm).

The spray cone angle, on the other hand, does not alter materially when the injection pressure changes. The maximum difference in spray cone angles among different injection pressures (Fig. 8) is less than 2° when the timing and ambient pressure are kept the same, and if plotted on the same axis (not shown here for brevity), there would be an obvious error bar overlap. This observation indicates that, for this injector, the liquid momentum is concentrated along the axial direction of the nozzles.

A closer look at the spray macroscopic parameters at 100 bar (Figs. 7 and 8(a)) and 200 bar (Figs. 7 and 8(c)) injection pressures reveals that their trends (with respect to the change of ambient pressures) of tip penetration length and spray cone angle are very similar to the one observed before at 150 bar injection pressure (Figs. 7 and 8(b), summarised in Table 1). Indeed, one could use the same three regions to describe the spray morphological behaviour at each injection pressure, albeit that the ambient-to-saturation pressure ratios at which the neighbouring regions separated may be different.

As summarised in Table 2, the maximum tip penetration length occurs at a lower ambient pressure when the injection pressure is higher. This is potentially due to a strengthened atomisation process at higher injection pressures. The increased momentum at higher injection pressures enhances the interaction between the spray and ambient gas, and based on previous findings for hydrocarbon sprays [34], this normally leads to finer droplets. Each of these smaller droplets has a larger surface-area-to-volume ratio and their trajectory is more sensitive to the change in ambient drag. In contrast, the strength of the flash boiling is mainly a function of ambient pressure, and it remains the same at various injection pressures. The combined result is visualised in Figs. 7 and 8 by an enlarged drag dominant region (green background) and a squeezed evaporation dominant region (blue background) at higher injection pressures.

The ambient pressure below which the spray collapse occurred (i.e., the "spray collapse point"), on the other hand, does not depend on the injection pressure. At all three injection pressures, the spray collapse phenomenon is observed only when $r_P \leq 0.23$ (≤ 2.0 bar ambient pressure, red background in Figs. 7 and 8). As discussed before in Fig. 8, the spray cone angle remains almost the same at different injection pressures, and this indicates that the extent of radial expansion of individual plumes may also remain unaltered when injection pressure is varied. As the spray collapse mechanism (discussed before) relies on adjacent plumes to be close enough to each other, if the individual plumes spanned similar radial distances, the injection pressure would not have a strong effect on when the spray collapse occurs. In fact, the spray collapse point would be more sensitive to hole pattern design.

4. Conclusions

Liquid anhydrous ammonia was injected from a repurposed multi-hole GDI injector into a constant volume chamber filled with nitrogen. The ambient (chamber) pressure varied 1 bar to 10 bar; the injection pressure was set to be 100 bar, 150 bar and 200 bar and the injection duration was 2 ms. Images of the resulting ammonia sprays were recorded at 10 kFPS by the diffuse backlit imaging technique. After post processing the images via a background subtraction algorithm, stationary chamber features were removed and spray plumes in each image were isolated. This enabled the computation of macroscopic spray parameters such as tip penetration length and spray cone angle following the SAE J2715 standard. The effects of ambient pressure and injection pressure on the morphological behaviour of ammonia sprays were examined, and the key findings are summarised below:

1. Ambient pressure (or its equivalent at a fixed saturation pressure, the ambient-to-saturation ratio r_P) has a profound effect on the morphological behaviour of ammonia sprays.

    (a) At high ambient pressures (large r_P), the plumes from each hole of the injector were separate and, due to higher drag from the quiescent ambient gases, the tip penetration lengths were shortened at higher ambient pressures, while the spray cone angles remained almost constant.

(b) At medium ambient pressures (medium r_P), despite the plumes still being separate, the flash boiling mechanism became more dominant than the effect of reduced drag. Stronger evaporation prevented the spray plumes from penetrating further and resulted in a reversed trend of tip penetration lengths — the tip penetration lengths were shorter at lower ambient pressures. In addition, the spray cone angle increased as the ambient pressure dropped. Within a given injection, the spray cone angle was steady throughout the duration of injection.

(c) At low ambient pressures (small r_P), spray collapse was observed and all plumes merged into a single plume immediately after they left their respective nozzles. The trend of tip penetration length for the merged plume was similar to those at higher ambient pressures — the plume penetrated further when ambient pressure dropped. On the other hand, the merged plume showed an unstable and unsteady behaviour in its radial expansion — the spray cone angle fluctuated under different ambient pressures and its value rapidly increased within a given injection (with respect to timing). Additionally, when ambient pressure was slightly higher, the six plumes firstly partially collapsed into two streams at earlier timings and merged to a single stream subsequently.

2. Spray morphology can be split into three regions, namely drag dominant (at high ambient pressures), evaporation dominant (at medium ambient pressures) and spray collapse (at low ambient pressures). At 150 bar injection pressure, the separation points between neighbouring regions were at $r_P = 0.53$ and $r_P = 0.23$, respectively. The latter is usually referred to the "spray collapse point".
3. Spray morphology is also influenced by injection pressure.

(a) Spray penetrated further at higher injection pressures owing to more momentum carried by the injected fluid.

(b) Spray cone angle remained almost constant (within ±1°) at different injection pressures. This indicates that the radial expansion of spray plumes are independent of injection pressure.

(c) The spray was more sensitive to the change in ambient drag when being injected at higher pressures, as a result of stronger dynamic breakup and enhanced interaction between the spray and ambient gas. The separation point between drag dominant and evaporation dominant shifted from $r_P = 0.59$ at 100 bar, to $r_P = 0.53$ at 150 bar and $r_P = 0.47$ at 200 bar injection pressures.

(d) However, the spray collapse point did not change when the injection pressure changed. For all three injection pressures tested, the point was at $r_P = 0.23$. This value is lower than those reported in the literature for hydrocarbon fuels, potentially due to the higher enthalpy of vaporisation of ammonia.

CRediT authorship contribution statement

Li Shen: Writing – original draft, Visualization, Validation, Software, Project administration, Methodology, Investigation, Formal analysis, Data curation, Conceptualization. **Felix Leach:** Writing – review & editing, Validation, Supervision, Project administration, Funding acquisition.

Declaration of competing interest

The authors declare that they have no known competing financial interests or personal relationships that could have appeared to influence the work reported in this paper.

Acknowledgement

This research was funded in whole or in part by Engineering & Physical Sciences Research Council (EPSRC, EP/V04673X/1). For the purpose of Open Access, the authors have applied a CC BY public copyright license to any Author Accepted Manuscript (AAM) version arising from this submission. Data supporting this paper is available from the "Oxford Research Archive" repository, accessible at https://ora.ox.ac.uk.

References

[1] Valera-Medina A, Xiao H, Owen-Jones M, David WIF, Bowen PJ. Ammonia for power. Prog Energy Combust Sci 2018;69:63–102.
[2] Faber Jasper, et al. Fourth IMO GHG study 2020 (full report). London: International Maritime Organization; 2021.
[3] The Royal Society. Ammonia: zero-carbon fertiliser, fuel and energy store. London: The Royal Society; 2020, Policy briefing.
[4] Senecal Kelly, Leach Felix. Racing toward zero: The untold story of driving green. Warrendale, PA: SAE International; 2021.
[5] The National Institute of Standards and Technology. NIST chemistry WebBook. 2023, NIST Standard Reference Database Number 69.
[6] Van Itterbeek A, Verbeke O, Theewes F, Staes K, De Boelpaep J. The difference in vapour pressure between normal and equilibrium hydrogen. Vapour pressure of normal hydrogen between 20K and 32K. Physica 1964;30(6):1238–44.
[7] Stull Daniel R. Vapor pressure of pure substances. Organic and inorganic compounds. Ind Eng Chem 1947;39(4):517–40.
[8] Ambalakatte Ajith, Cairns Alasdair, Geng Sikai, Varaei Amirata, Hegab Abdelrahman, Harrington Anthony, Hall Jonathan, Bassett Michael. Experimental comparison of spark and jet ignition engine operation with ammonia/hydrogen co-fuelling. In: WCX SAE world congress experience. 2024-01-2099, SAE International; 2024.
[9] Min Chan ki, Lee Seung Woo, Baek Hong-Kil. Development of ammonia direct injection 4-cylinder spark-ignition engine. In: WCX SAE world congress experience. 2024-01-2818, SAE International; 2024.
[10] Reggeti Shawn A, Kane Seamus P, Northrop William F. Hydrogen production in ammonia-fueled spark ignition engines. Appl Energy Combust Sci 2023;14:100136.
[11] Zhang Zhifei, Li Tie, Chen Run, Wang Ning, Wei Yijie, Wu Dawei. Injection characteristics and fuel-air mixing process of ammonia jets in a constant volume vessel. Fuel 2021;304:121408.
[12] Stone Richard. Introduction to internal combustion engines. 4th ed.. London: Red Globe Press; 2012.
[13] Leach Felix, Ismail Riyaz, Davy Martin. Engine-out emissions from a modern high speed diesel engine – The importance of nozzle tip protrusion. Appl Energy 2018;226:340–52.
[14] Li Xuesong, Wang Shangning, Yang Shangze, Qiu Shuyi, Sun Zhe, Hung David LS, Xu Min. A review on the recent advances of flash boiling atomization and combustion applications. Prog Energy Combust Sci 2024;100:101119.
[15] Xu Min, Zhang Yuyin, Zeng Wei, Zhang Gaoming, Zhang Ming. Flash boiling: Easy and better way to generate ideal sprays than the high injection pressure. SAE Int J Fuels Lubr 2013;6(1):137–48.
[16] Sher Eran, Bar-Kohany Tali, Rashkovan Alexander. Flash-boiling atomization. Prog Energy Combust Sci 2008;34(4):417–39.
[17] Chang Mengzhao, Lee Ziyoung, Park Sungwook, Park Suhan. Characteristics of flash boiling and its effects on spray behavior in gasoline direct injection injectors: A review. Fuel 2020;271:117600.
[18] Guo Hengjie, Li Yanfei, Lu Xinhui, Zhou Zhifu, Xu Hongming, Wang Zhi. Radial expansion of flash boiling jet and its relationship with spray collapse in gasoline direct injection engine. Appl Therm Eng 2019;146:515–25.
[19] Ahmed Noor A. Coanda effect: Flow phenomenon and applications. 1st ed.. Boca Raton: CRC Press; 2019.
[20] Zeng Wei, Xu Min, Zhang Gaoming, Zhang Yuyin, Cleary David J. Atomization and vaporization for flash-boiling multi-hole sprays with alcohol fuels. Fuel 2012;95:287–97.
[21] Huang Yuhan, Huang Sheng, Huang Ronghua, Hong Guang. Spray and evaporation characteristics of ethanol and gasoline direct injection in non-evaporating, transition and flash-boiling conditions. Energy Convers Manage 2016;108:68–77.
[22] Oh Heechang, Hwang Joonsik, White Logan, Pickett Lyle M, Han Donghee. Spray collapse characteristics of practical GDI spray for lateral-mounted GDI engines. Int J Heat Mass Transfer 2022;190:122743.
[23] Pelé Ronan, Mounaïm-Rousselle Christine, Bréquigny Pierre, Hespel Camille, Bellettre Jérôme. First study on ammonia spray characteristics with a current GDI engine injector. Fuels 2021;2(3):253–71.
[24] Cheng Qiang, Ojanen Katriina, Diao Yantao, Kaario Ossi, Larmi Martti. Dynamics of the ammonia spray using high-speed schlieren imaging. SAE Int J Adv Curr Pr Mobil 2022;4(4):1138–53.

[25] Colson Sophie, Yamashita Hirofumi, Oku Kohei, Somarathne Kapuruge Don Kunkuma Amila, Kudo Taku, Hayakawa Akihiro, Kobayashi Hideaki. Study on the effect of injection temperature and nozzle geometry on the flashing transition of liquid ammonia spray. Fuel 2023;348:128612.

[26] Fang Yuwen, Ma Xiao, Zhang Yixiao, Li Yanfei, Zhang Kaiqi, Jiang Changzhao, Wang Zhi, Shuai Shijin. Experimental investigation of high-pressure liquid ammonia injection under non-flash boiling and flash boiling conditions. Energies 2023;16(6):2843.

[27] Li Shiyan, Li Tie, Wang Ning, Zhou Xinyi, Chen Run, Yi Ping. An investigation on near-field and far-field characteristics of superheated ammonia spray. Fuel 2022;324:124683.

[28] Shen Li, Leach Felix. Effect of ambient pressure on ammonia sprays using a single hole injector. In: WCX SAE world congress experience. 2024-01-2618, SAE International; 2024.

[29] Mohd Murad Safwan Hanis, Camm Joseph, Davy Martin, Stone Richard, Richardson Dave. Spray behaviour and particulate matter emissions with M15 methanol/gasoline blends in a GDI engine. In: SAE 2016 world congress and exhibition. 2016-01-0991, SAE International; 2016.

[30] Leach Felix, Stone Richard, Fennell Derek, Hayden David, Richardson Dave, Wicks Nick. Predicting the particulate matter emissions from spray-guided gasoline direct-injection spark ignition engines. Proc Inst Mech Eng Part D: J Automob Eng 2017;231(6):717–30.

[31] SAE Gasoline Fuel Injection Standards Committee. Gasoline fuel injector spray measurement and characterization. vol. SAE Standard J2715, SAE; 2007.

[32] Hung David LS, Harrington David L, Gandhi Anand H, Markle Lee E, Parrish Scott E, Shakal Joseph S, Sayar Hamid, Cummings Steven D, Kramer Jason L. Gasoline fuel injector spray measurement and characterization – A new SAE J2715 recommended practice. SAE Int J Fuels Lubr 2009;1(1):534–48.

[33] Desclaux Anthony, Pelé Ronan, Hespel Camille, Mounaïm-Rousselle Christine. Liquid ammonia injection on single hole injector: effect of initial conditions on flash boiling process. In: 32nd European conference on liquid atomization and spray system. Ffhal-04211267, ILASS Europe 2023; 2023.

[34] Hawi Meshack, Kosaka Hidenori, Sato Susumu, Nagasawa Tsuyoshi, Elwardany Ahmed, Ahmed Mahmoud. Effect of injection pressure and ambient density on spray characteristics of diesel and biodiesel surrogate fuels. Fuel 2019;254:115674.